Available online at www.sciencedirect.com

ScienceDirect

journal homepage: www.elsevier.com/locate/he

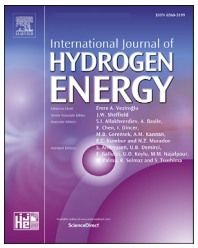

One step fabrication of nanostructured nickel thin films on porous nickel foam for drastic electrocatalytic oxygen evolution

Muhammad Ali Ehsan [a,*], *Zaka Ullah* [b], *Muhammad Faizan Nazar* [c], *Muhammad Younas* [d], *Munzir Suliman* [a]

[a] *Interdisciplinary Research Center for Hydrogen and Energy Storage (IRC-HES), King Fahd University of Petroleum & Minerals, Box 5040, Dhahran 31261, Saudi Arabia*

[b] *Department of Physics, Division of Science and Technology, University of Education, Lahore, 54770, Pakistan*

[c] *Department of Chemistry, Division of Science and Technology, University of Education, Lahore, 54770, Pakistan*

[d] *Core Research Facilities, King Fahd University of Petroleum and Minerals, Dhahran 31261, Saudi Arabia*

HIGHLIGHTS

- Single-step chemical vapor deposition of nickel thin film on porous nickel foam.
- Changing deposition time affects thin film microstructure.
- Investigation of nickel electrocatalyst for water oxidation in alkaline medium.
- Nickel film fabricated for 60 min exhibits remarkable oxidation activity.
- Nickel film electrocatalyst remains highly stable during electrochemical operation.

ARTICLE INFO

Article history:
Received 13 November 2022
Received in revised form
4 January 2023
Accepted 7 January 2023
Available online 28 January 2023

Keywords:
Thin film
Nickel metal
Nickel foam
Oxygen evolution
Electrocatalyst
Deposition time

ABSTRACT

The oxygen evolution reaction (OER) is crucial for sustainable hydrogen production through competitive water electrocatalysis. In this work, nanostructured nickel (Ni) thin films deposited on porous nickel foam (NF) substrate are investigated for improved OER catalysis in alkaline medium. The time-dependent fabrication of Ni thin films is achieved via aerosol-assisted chemical vapor deposition (AACVD), which has shown promising impact on the OER performance. Particularly, the nanoscale Ni@NF electrocatalyst after 60-min of deposition showed outstanding OER properties including minimum overpotential of 285 and 423 mV to reach the current decade (10 $mAcm^{-2}$) and even higher than 1000 mA/cm^2, respectively. The electrode exhibits a small Tafel slope with a value of 70 mV dec^{-1}, a higher TOF, a large electrochemically active surface area, better charge transport performance, and long-term stability over 20 h of continuous operation without significant loss. This OER catalytic activity for pristine Ni electrocatalysts is a significant milestone and is found much better than the benchmark noble metal OER catalysts as well as many other well-known 3D transition metal catalysts. The impressive OER performance is attributed to the synergic effect generated between nanostructured-Ni and porous NF substrate, which enhances the electrical conductivity of the designed catalysts. The low manufacturing cost, robustness, and durability make this catalyst viable in solar energy conversion and storage applications.

* Corresponding author.
E-mail address: meali@kfupm.edu.sa (M.A. Ehsan).

https://doi.org/10.1016/j.ijhydene.2023.01.083

Introduction

Hydrogen is an efficient energy carrier with great potential for clean and sustainable energy in future applications [1,2]. However, the sustainable and renewable character of hydrogen mainly depends upon its production strategy. Currently, hydrogen production is dominated by methane steam reforming and coal gasification processes, which are associated with significant CO_2 emissions [3–5]. In addition, the COVID-19 pandemic has shown the strain on centralized oxygen delivery systems and the importance of portable and reliable oxygen supplies [6]. To address these challenges, electrocatalytic water splitting represents a promising alternative to achieve clean and pure hydrogen and oxygen through two half-cell reactions called hydrogen evolution reaction (HER) and oxygen evolution reaction (OER) [1,7,8].

The water splitting process mainly relies on OER as it provides the necessary protons and electrons to achieve the target reduction. However, the slower kinetics of OER is the bottleneck of water electrolysis and is crucial to improve the efficiency of the entire electrochemical conversion process [9,10]. To accelerate the OER rate, highly active and conductive platinum group (PGM) metals such as Pt, Ir, and Ru are used as electrocatalysts, which make the water splitting process very expensive and impractical for commercial-scale hydrogen production [11–15]. The PGM electrocatalysts are inherently capable of water oxidation under acidic/neutral environments as these are the designated candidates for contemporary polymer electrolyte membrane (PEM) electrolyzers. However, the expensiveness and scarcity of these catalytic materials has prompted the search for proficient electrocatalysts made up of cheap and readily available elements as sustainable and economically viable alternatives.

Electrocatalytic materials based on 3D transition elements (Mn, Fe, Co, and Ni) have emerged as favorable choices to PGMs for water oxidation processes [16–19]. In particular, Ni-based electrocatalysts have become increasingly important due to excessive electrical conductivity, high stability, and corrosion resistance characteristics under alkaline conditions [20,21]. Recently, a wide variety of advanced nickel compounds have been explored for OER electrocatalysis, of which some notable examples are discussed here. For example, X. Yan et al. synthesized defects-rich nickel nanoparticles by a hydrothermal method and found that the materials are better catalysts for the electro-oxidation of urea compared to that of ordinary metallic nickel [22]. H. H. El-Maghrabi and co-workers designed Ni/NiO–TiO_2/rGO nanocomposites on carbon cloth conductor by plasma-enhanced chemical vapor deposition. The catalyst showed high catalytic activities and long-term stability for electrocatalytic water oxidation [23]. Nickel oxide nanoparticles prepared by chemical precipitation method on graphite planes [NiO/Gt] had performed urea oxidation in fuel cells at significantly high rates [24]. Mesoporous NiO catalysts with different morphology were synthesized by hydrothermal methods, and the nanoplate-nanorod catalyst showed high porosity and better electrocatalytic activity for OER than other samples [25]. Highly porous and honeycomb-like structures based on nickel oxide catalysts have been readily electro-deposited onto multi-walled carbon nanotubes for low overpotential water oxidation [26]. A Ni/C catalyst, prepared by polyol method has been thoroughly characterized and tested for the electro-oxidation of lignin and 2-phenoxyethanol [27]. Also, nickel/nickel oxide on reduced graphene oxide (Ni/NiO@rGO) [28], nickel oxide nanosheets array on carbon cloth (NiO NA/CC) [29], nickel-nickel oxide nanoparticles embedded in carbon nanofibers (Ni–NiO/C) [30], assembly of selenium-doped nickel nanosheets [31], and self-assembled nickel oxide nanoflakes [32] have been reported as highly efficient catalysts for electrochemical water oxidation.

Several general synthetic methods including sol-gel [33], pulsed laser deposition [34], electrodeposition [35], sputtering [36], and chemical vapor deposition [37] have been used to fabricate Ni-based anodes with higher activity in OER catalysis. Despite the excellent OER catalytic activity observed in these studies, the synthesis involves multiple steps and hour-long processing with serious deficiencies in reproducibility and homogeneity, making them unattractive for large-scale industrial manufacturing. Here, we report an accessible and accelerated deposition route to develop metallic Ni films using aerosol-assisted chemical vapor deposition (AACVD) technique, through which a batch of films with different thicknesses and morphologies can be produced in a very short time. AACVD also allows the use of highly conductive and porous metal substrates such as Fe, Ni, and Cu foams as catalyst supports, which is advantageous for reducing resistance between electrodes/electrocatalysts [38,39]. The nanomaterials developed directly on 3D conductive substrates facilitate the mass diffusion and surface catalysis. Notably, NF with 3D porous structure is beneficial for electrolyte permeation and bubbles release, along with the promotion of mass transport for the reactants, which ultimately improves catalytic activity [40–42]. In particular, metal-based supports can directly contribute to improve the overall performance of electrocatalysts. In the present work, metallic Ni films were deposited on 3D Ni-foam for 30, 60, and 120 min and examined for OER activity. The Ni@NF electrode prepared in 60 min provided very high OER performance with an overpotential of 285 mV at 10 mA/cm and continued to perform the OER for more than 20 h without significant loss.

Experimental

Preparation of metallic nickel electro catalysts

The preparation of Ni films was achieved using AACVD equipment and method mentioned in our previous report [43]. Compared to previous work, two deposition parameters were changed, namely, porous nickel foam (NF) was used as the substrate material, and the deposition time was extended for some longer time (~2 h). Whereas, precursor nickel (II) acetylacetonate ($Ni(acac)_2$), deposition solvent (methanol), deposition temperature (500 °C) and carrier gas/flow rate (N_2 gas (150 cm^3/min) remained the same. Films growth time intervals

were 30, 60 and 120 min, and the thin film electrodes were named as Ni@NF-30, Ni@NF-60 and Ni@NF-120, respectively.

Electrocatalyst characterization

Electrocatalytic Ni thin films were investigated through various characterizations. X-ray diffraction (XRD) pattern was measured using a Rigaku MiniFlex X-ray diffractometer (Japan) with a Cu Kα1 source ($\gamma = 0.15416$ nm). Scanning electron microscope (SEM) JEOL JSM-6610LV (Japan) was used for morphological characterization of the samples. The elemental composition of the films was determined by energy-dispersive X-ray spectroscopy (EDX, INCA Energy 200, Oxford Instruments, UK). TEM measurement analysis was employed using JEOL-JEM2100F, Japan, functioned at an accelerating voltage of 200 kV. The specific oxidation and chemical states of deposited nickel were determined by X-ray photoelectron spectroscopy (XPS) performed on a Thermo Scientific Escalab 250Xi spectrometer equipped with a monochromatic Al Kα (1486.6 eV) X-ray source of 0.5 eV resolution. For charge correction, the data were calibrated against C (1s) random carbon (284.8 eV) and the peaks were modeled with Casa XPS software.

Electrochemical water oxidation investigations

Electrochemical water oxidation tests were performed in 1.0 M KOH electrolyte solution at pH 14. Typical cell with three electrodes consisted of Ni@NF catalyst (working electrode), Ag/AgCl (reference electrode), and Pt wire (counter electrode), connected to a computer-controlled potentiostat INTERFACE 1010 E. All electrochemical measurements were performed in a deoxygenated electrolyte aqueous solution at room temperature. Polarization curves were recorded using linear sweep voltammetry at a scan rate of 2 mV/s, as mentioned elsewhere. All potentials here are converted to reversible hydrogen electrodes (RHE) according to the Nernst equation:

$$E_{RHE} = E_{REF} + E^{0}_{REF} + 0.059\ (pH)$$

The overpotential is calculated according to the following formula:

$$\text{Overpotential } (\eta) = E_{RHE} - 1.23$$

The Tafel slope is calculated from the linear region of the polarization curve (where the Tafel region begins) using the Tafel equation:

$$\eta = b \log j + a$$

where "b" defines Tafel slope while "a" is constant.

Results and discussions

Structural properties of nanostructured nickel films

Metallic nickel (Ni) thin films deposited by AACVD on Ni-foam substrate were characterized by XRD. Coincidentally, the crystalline peaks of AACVD-deposited Ni merged into the XRD peaks of Ni from NF. Three high-intensity peaks were observed at the 2θ positions of 44.7, 51.8, and 76.6° on the respective reflective surfaces (111), (200), and (220), evidencing the existence of a cubic-structured "metallic nickel" (PDF # 01-077-8341) [43]. To verify this observation, AACVD experiments were repeated on simple amorphous glass substrate. Fig. 1 shows the XRD patterns of these films, which are in perfect agreement with the XRD results obtained on NF substrates.

The surface morphology of nickel deposited by AACVD on NF substrates after a 30–120 min deposition process was analyzed by scanning electron microscopy (Fig. 2). Bare NF has a smooth and featureless texture, while showing well-defined grain boundaries, as shown in low and high-resolution SEM images in Fig. 2(a and b). The effects of deposition time from 30 to 120 min in the form of widely deposited material can be seen in the low-resolution images (Fig. 2(c, e, g)). The corresponding high-resolution images reveal details of the shape and texture of the deposited nickel. The first 30 min of deposition produced many nanoscale objects (Fig. 2(d)), which continued to grow and transform into snowflakes like objects as the sintering time was increased to 60 min (Fig. 2(f)). The sintering effect became very apparent when the immediate 120 min deposition showed that the particles coalesced and formed compact and dense patterns.

The change in morphology in such a short time is a defining feature of AACVD, which provides a variety of nanostructure designs and thicknesses and determines the catalytic performance of each material towards better performance [44,45]. Furthermore, the deposited species are strongly bound to the NF, and the resulting thin-film electrodes are easily used for electrochemical demonstrations

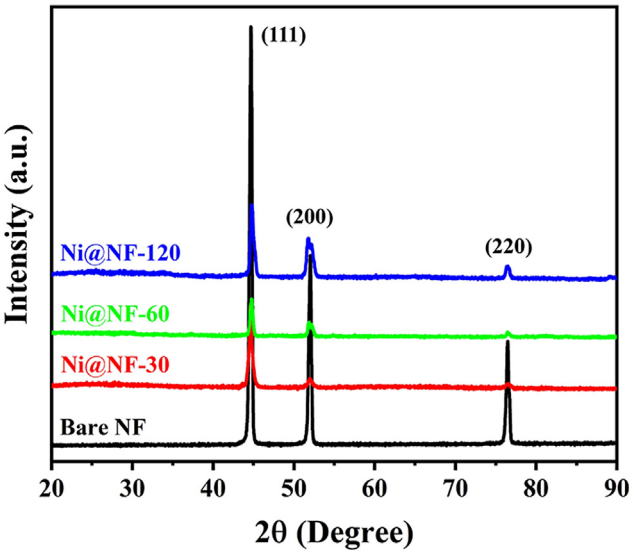

Fig. 1 – XRD overlays of cubic Ni thin films deposited by AACVD on common glass substrates at different deposition times of 30 min (red line), 60 min (green line) and 120 min (blue line) while black line represents the bare nickel foam pattern. (For interpretation of the references to color in this figure legend, the reader is referred to the Web version of this article.)

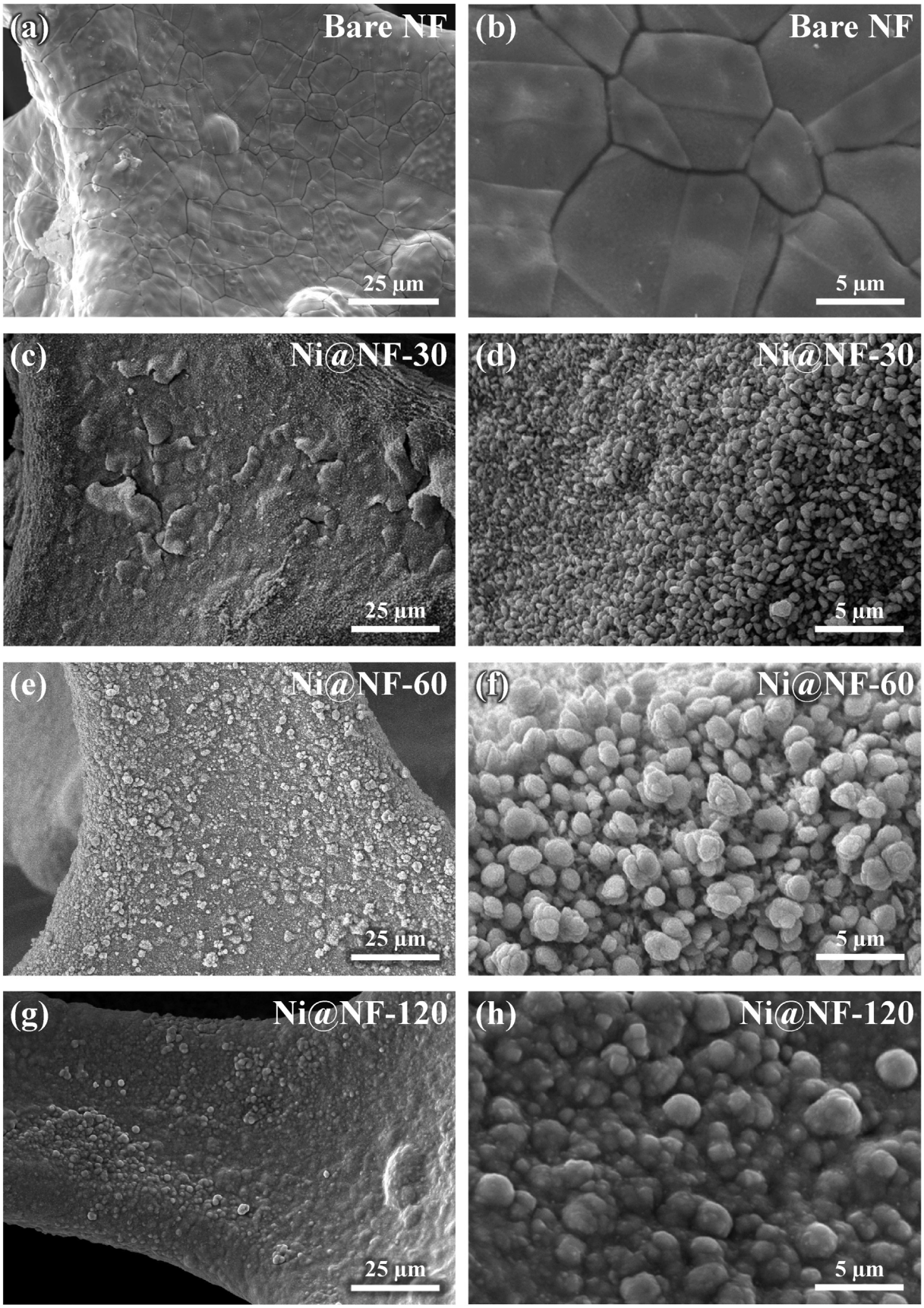

Fig. 2 – Low-resolution (left column) and high-resolution (right column) SEM images of Ni thin films deposited on nickel foam at different deposition time: (a, b) 0 min, (c, d) 30 min, (e, f) 60 min and (g, h) 120 min.

without further thermal or mechanical treatments. The elemental composition of the nickel thin film catalyst was investigated by energy dispersive X-ray (EDX) analysis and the results are presented in Fig. S1. All EDX spectra show the presence of only nickel element in these samples. No peak associated with oxygen atom is observed, suggesting the formation of pure metallic Ni in all three samples.

Further the morphology and crystalline structure of Ni@NF-60 catalyst was analyzed by transmission electron microscope (TEM). The size of nickel nano-flakes measured from TEM micrographs (Fig. 3(a) and (b)), exist in the range of 20–40 nm and many nano-crystallites are stacked together. The high-resolution TEM image (Fig. 3(c)), reveals the numerous fringes on the surface of the nano-crystallite. The inter-planar distance (*d*-spacing) measured from many random places is found to be constant (0.21 nm), which agrees well with the *d*-spacing value (0.20 nm) observed for the 100% intensity peak (111) of cubic phased "Ni" from XRD pattern. In addition, the typical diffraction rings in the selected area electron diffraction (SAED) pattern (Fig. 3(d)) demonstrate the polycrystalline nature of the Ni thin film catalyst.

X-ray photoelectron spectroscopy (XPS) was used to determine the specific oxidation and chemical state of nickel deposited by AACVD. Consequently, nickel film deposited on ordinary glass was used. Survey scan spectrum indicates the presence of mandatory Ni element on the film surface (Fig. 4(a)). Besides, multiple peaks originated from glass elements (Br, Sn, Na, Ba) have been observed and labelled accordingly, as shown in Fig. 4(a). The high-resolution Ni 2p spectrum is shown in Fig. 4(b), wherein the black curve indicates the experimental data, which is further deconvoluted and represented by multi-colored lines. The two sets of broad signals, corresponding to Ni 2p3/2 (~853 eV) and Ni 2p1/2 (~870 eV), and two satellite peaks indicating, the zero oxidation state of Ni [46,47].

OER electrocatalysis

The electrocatalytic OER performance of nanostructured Ni films deposited on Ni-foam substrates (Ni@NF) was evaluated in 1.0 M KOH electrolyte medium. Cyclic voltammetry (CV) tests were primarily performed to observe the I–V behavior of thin-film electrodes over a range of applied potential (0.0–0.8 V vs. NHE). Initial CV experiments provide important insights about the chemical and mechanical stability of electrocatalysts under the applied electrochemical conditions. Recent work has established that the continuous CV scans develop high oxidative electroactive spices on the surface of Ni based catalyst, which expedites the kinetics of water oxidation reaction [48–51].

Initially, all three Ni electrocatalysts were activated by conducting simultaneous fifty (50) CVs at the rate of 50 mV/s. Bare NF was also tested in similar environment to observe its contribution in the activation process. Fig. 5 (a)-(d) indicates a comparative overview of 1st and 50th CV cycle of all Ni electrocatalysts and bare NF. A significant improvement in CV response can be seen as a result of repeated CV sweeps. In particular, the 50th CV curve shows a high-amplitude anodic peak at ~0.40 V *vs* NHE for all catalytic systems followed by a steep catalytic current from water oxidation. Whereas, in the cathodic run there is a broad peak centered at ~0.30 V, which is assigned to the reduction of surface deposits formed in the initial anodic scan. These redox peaks are relatively very weak in the 1st CV cycle. Repetitive CV scans show that the onset

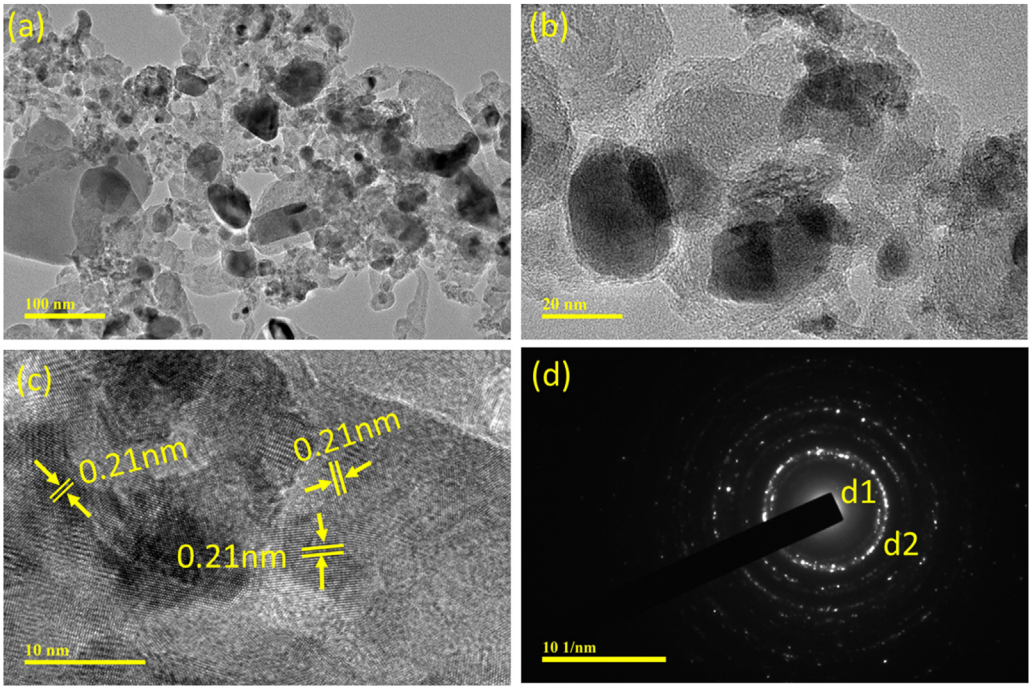

Fig. 3 – TEM analysis of Ni@NF-120 catalyst: (a) Low-resolution and (b) high resolution TEM images. (c) HR-TEM at 10 nm presenting the lattice fringes of Ni. (d) SAED showing the ring formation for a polycrystalline nature of Ni, while d1 and d2 correspond to the (111) and (200) *hkl* reflection planes, respectively.

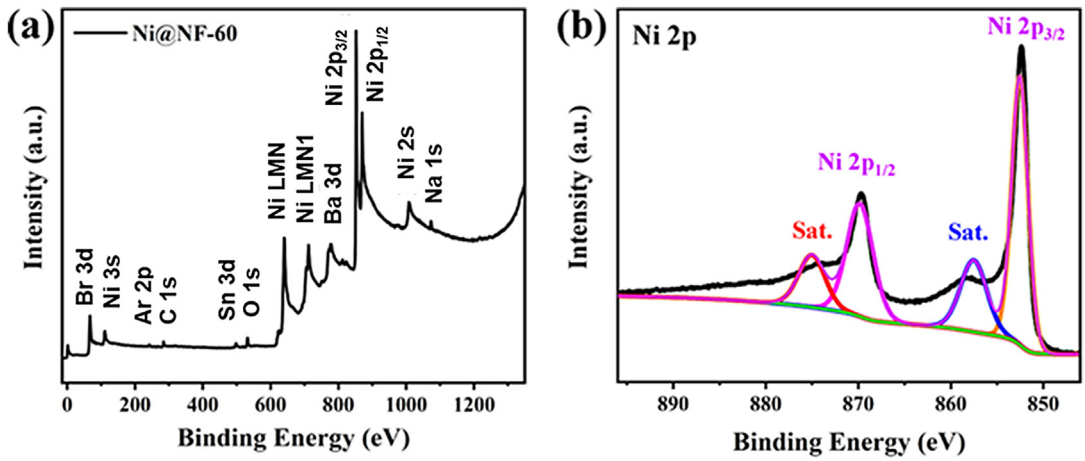

Fig. 4 – XPS spectrum of nickel film deposited on common glass substrate: (a) survey scan and (b) high-resolution deconvoluted spectrum of Ni representing the zero oxidation state. The black line indicates the experimental data, while multi-color lines show the fitted data. (For interpretation of the references to color in this figure legend, the reader is referred to the Web version of this article.)

potential of water oxidation is shifted toward the cathode, while the cathodic peak is shifted toward the anode. The catalytic current density and the amplitude of the anodic peak increased with the scan, indicating the growth of electroactive fragrances on the film surface. However, in the case of bare NF (Fig. 5(a)), the water oxidation current density is very low compared to the nanostructured nickel deposition catalyst, which confirms low activation of NF as a result of concurrent CV scans.

Following CV experiments, linear sweep voltammetry (LSV) or polarization curves were recorded for all electroactive catalysts in 1.0 M KOH and at a scan rate of 2 mV/s. Fig. 6(a)

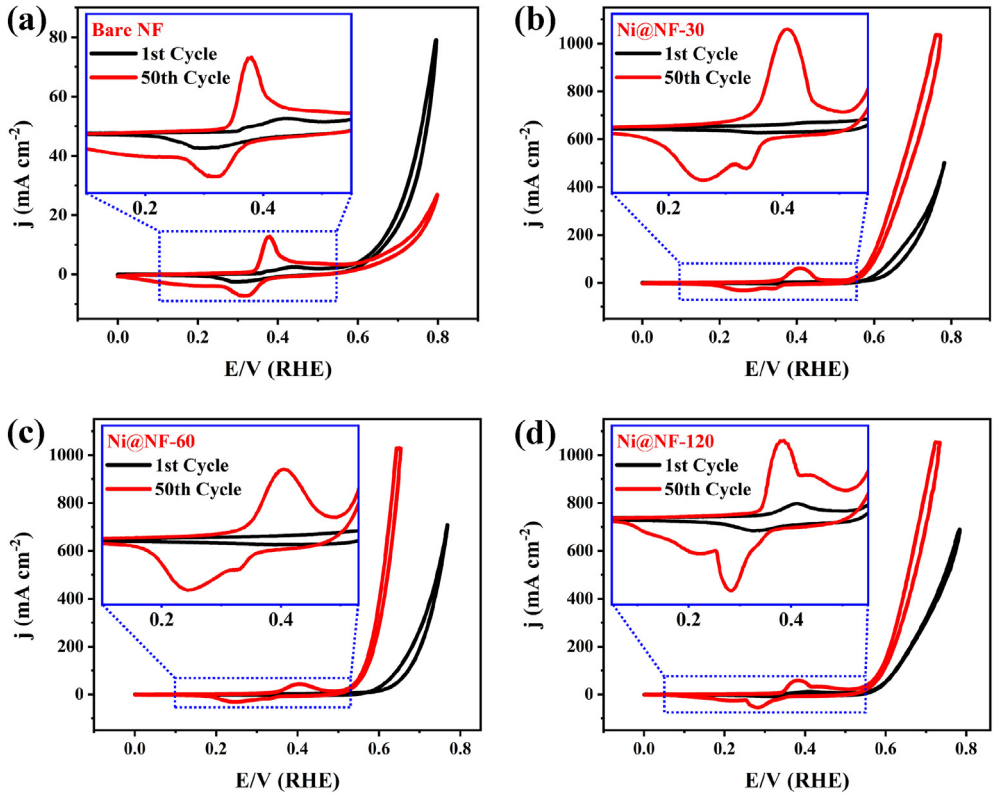

Fig. 5 – Electrocatalytic OER characterization of various Ni@NF catalysts and comparison of 1st and 50th continuous CV scan. (a) Bare NF, (b) Ni@NF-30, (c) Ni@NF-60 (d) Ni@NF-120 in 1.0 M KOH electrolyte solution at a scan rate of 50 mV s^{-1}. The corresponding insets show the anodic and cathodic peak behavior for each catalyst.

shows the comparative LSV curves of all catalytic systems, namely Bare NF, Ni@NF-30, Ni@NF-60 and Ni@NF-120. The polarization curves definitely indicate the excellent OER performance of the nanostructured Ni@NF catalyst deposited by AACVD. In all three cases, water oxidation starts at a very low onset potential (1.5 V vs. RHE), and the water oxidation current approaches the highest current density of >1000 cm^{-2}, reflecting the tremendous OER activity of the as-synthesized Ni electrocatalysts. This behavior is highly favorable for OER catalysts, which corresponds to a faster heterogeneous electron transfer progression at the active surface [52]. The bare NF based catalyst showed only a small increase in current, implying that NF contributed little to the catalytic activity, and suggested that the nanostructured Ni film was mainly responsible for the OER performance.

All electrocatalysts showed peak currents at between 1.35 and 1.40 V vs RHE due to the oxidation of Ni^{2+} to Ni^{3+} for generation of NiOOH, which may be active intermediates for OER (Fig. 6(b)). To avail 10 mA cm^{-2}, the Ni@NF-60 catalyst requires a minimum overpotential of 280 mV, while Ni@NF-30 and Ni@NF-120 require slightly higher overpotentials of ~300 mV. When comparing the catalytic performance at 1000 mA/cm^2, Ni@NF-60 consumes less overpotential (423 mV) than the other two catalytic systems that consume 506 mV overpotential, yet offer similar OER activity. Overall, the OER performances of the nanostructured Ni@NF electrodes are comparable to each other, which indicates that the sintering effect and mass loading have very little influence on the catalytic activity, and the synergistic effect of the nanostructured AACVD-derived Ni and NF substrates in all three cases prevails.

Tafel analysis was performed to evaluate the intrinsic kinetics of the developed electrocatalysts. As shown in Fig. 6(d), the OER Tafel slope (73 mV dec^{-1}) of the Ni@NF-60 catalyst is significantly lower than that of Ni@NF-30 (96 mV dec^{-1}), Ni@NF-120 (101 mV dec^{-1}) and bare NF (183 mV dec^{-1}), showing the improved oxygen evolution kinetics of Ni@NF-60. The Tafel slope values for the 30-min and 120-min electrodes are nearly identical, indicating comparable OER kinetics behavior. As a comparison, Tafel slope values in alkaline media for many well-known OER catalysts such as Pt [53] and NiCo, CoCo-layered double hydroxides [54] are reported in the range of 60–65 mV/dec. For Ni-based OER catalysis, Tafel slope values above 60 mV/dec indicate the dominance of the electroactive spice NiOOH, while higher slopes of 120 mV/dec indicate that the adsorbed Ni–O is the catalytic surface predominant [55]. In this example, the nanostructured Ni indicates the existence of kinetic conditions dominated by adsorbed NiOOH, leading to higher current densities.

Further, EIS measurements were performed to reveal the interfacial behavior and the intrinsic OER activity of the as-synthesized Ni@NF electrodes. Fig. 7(a) shows the EIS Nyquist plot, with smaller EIS arcs reflecting lower interfacial charge transport barriers and better electrocatalyst

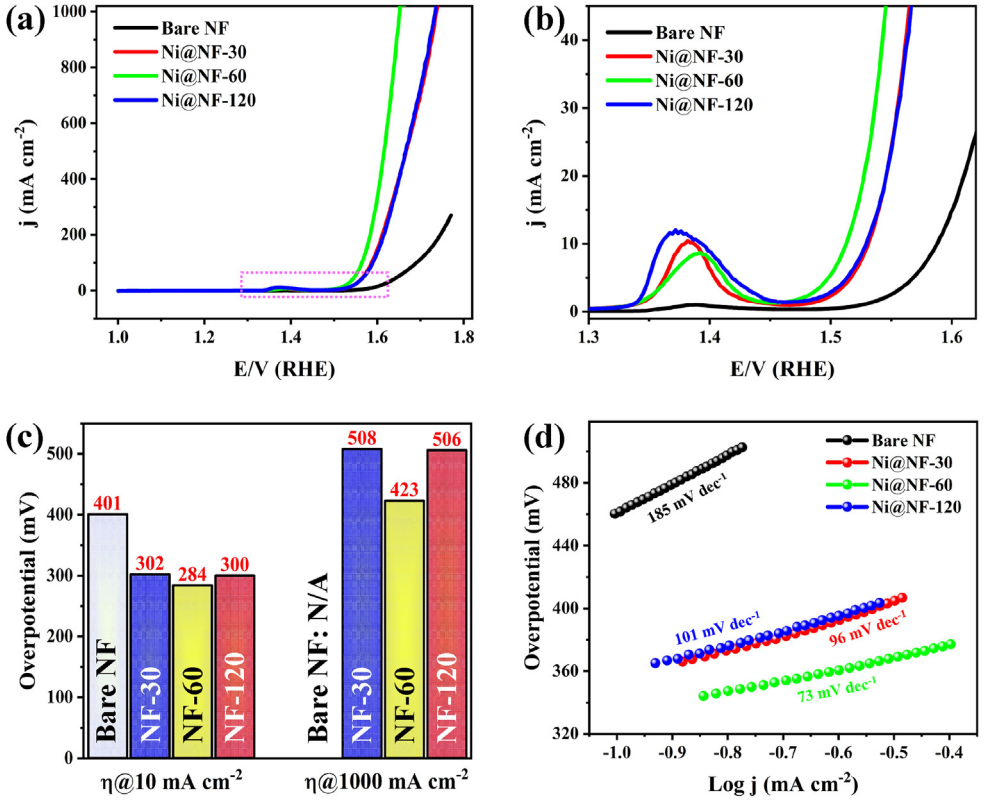

Fig. 6 – Electrocatalytic OER studies: (a) polarization curves of different Ni@NF electrocatalysts deposited in 1.0 M KOH electrolyte solution. The curves are recorded at a scan rate of 2 mV/s for all the prepared samples. (b) Inflated view of part (a). (c) Onset overpotential values for different as-developed electrodes. (d) Tafel plots and corresponding Tafel slope values for bare NF and as-developed nickel catalysts on NF at distinctive deposition times.

conductivity. Based on these criteria, the Ni@NF-60 electrocatalyst exhibits lower elasticity and better charge transport performance compared to the other two electrocatalysts, thus showing leading OER activity. Moreover, Ni@NF-60 manifests a smaller charge transfer resistance (R_{ct}) value of 120 Ω. Whereas, Ni@NF-30, Ni@NF-120 and bare NF show R_{ct} of 320, 350 and 470 Ω, respectively (Fig. 7(a): Randles circuits are fitted to study charge transfer resistance values, as presented in the inset of Fig. 7(a)). Furthermore, turnover frequency (TOF) was calculated to evaluate the intrinsic catalytic activity of these electrocatalysts. The TOF value is derived from the following formula:

$$TOF = \frac{j \times A}{4 \times F \times m}$$

In the above relation, j represents the current density and it was measured at an overpotential of 350 mV in A cm^{-2}). A is the surface area of NF substrate (1 cm^{-2}), F is the Faraday constant (96,485 C mol^{-1}) and m is the number of moles of catalyst deposited on the NF substrate. The mass of as-synthesized electrocatalysts Ni@NF-30, Ni@NF-60, and Ni@NF-120 was 0.08, 0.23, and 0.46 mg, respectively. The TOF values of Ni@NF electrocatalysts at different overpotentials are directly calculated from the polarization curves, as shown in Fig. 7(b). The TOF values measured at 350 mV for Ni@NF-30, Ni@NF-60, and Ni@NF-120 are 0.05 s^{-1}, 0.3 s^{-1} and 0.25 s^{-1}, respectively. The higher TOF value of the Ni@NF-60 electrode differentiates it from other Ni@NF electrocatalysts for OER with improved kinetics.

Since, Ni@NF-60 exhibited impressive OER activity and kinetics, the long-term stability of the catalyst was further tested to verify its suitability for large-scale applications. Long-term electrolysis was performed by chronopotentiometry by applying respective current density of 10 and 20 mA/cm^2 for 20 h. Due to the applied current density, a stable linear response was obtained, confirming the long-term stability of Ni@NF-60 throughout the OER process. When 10 mA/cm^2 was applied, an overvoltage value of 300 mV was initially observed, which remained constant for the first 10 h. With the increase in current density from 10 to 20 mA/cm^2, the overpotential shifted slightly from 300 mV to 312 mV and remained almost unchanged for the next 10 h.

Robustness is a property that demonstrates the *in situ* activation of the catalyst and the creation of an increasing number of electroactive sites on the catalyst surface during long-term OER testing under alkaline conditions. The results also showed that the overvoltage remained almost constant at the two distinctive applied current densities without any obvious drop in its value. Likewise, no signs of deterioration or detachment of the electrodes were observed in the long-term stability test. This is one of the significant advantages of thin film electrocatalysts over powder electrocatalysts; the catalyst does not separate during electrochemical studies. Moreover, Ni@NF-60 catalyst has capability to perform OER even at

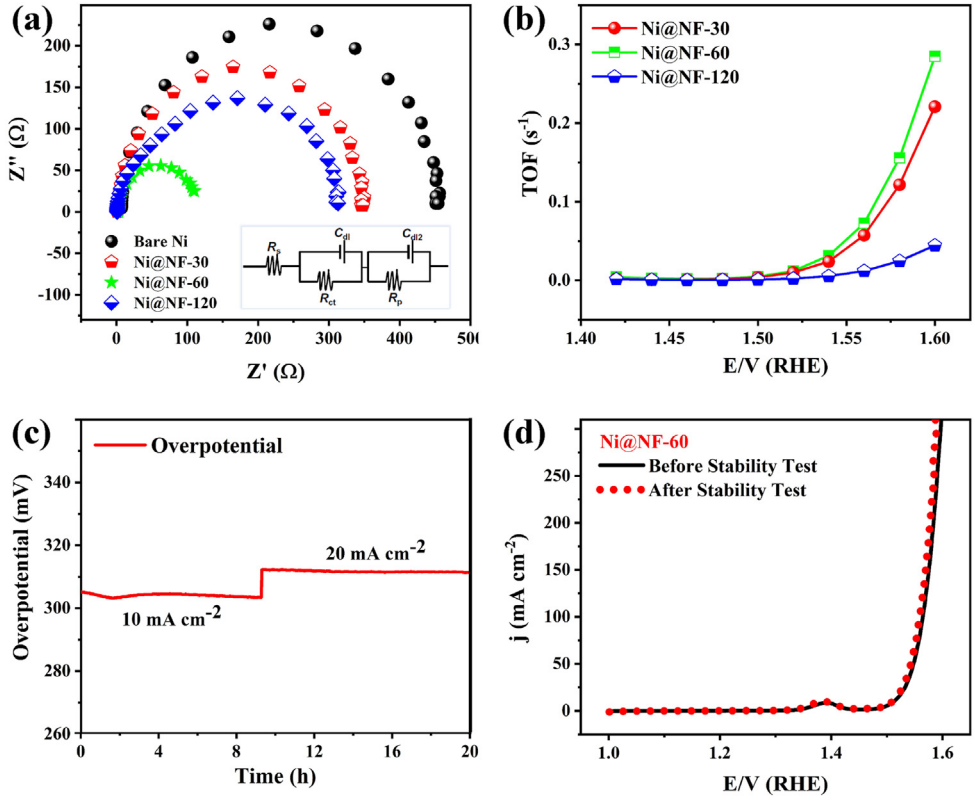

Fig. 7 – Electrocatalytic OER investigations: (a) EIS Nyquist plots for different Ni@NF electrocatalyst and inset showing the Randles circuit fitting. (b) TOF values of all Ni@NF systems extracted from corresponding polarization curves. (c) Chronopotentiometry long term OER response of Ni@NF-60 catalyst conducted at two different applied current densities of 10 and 20 mA/cm^2. (d) Polarization curves of Ni@NF-60 catalyst before and after chronopotentiometric study.

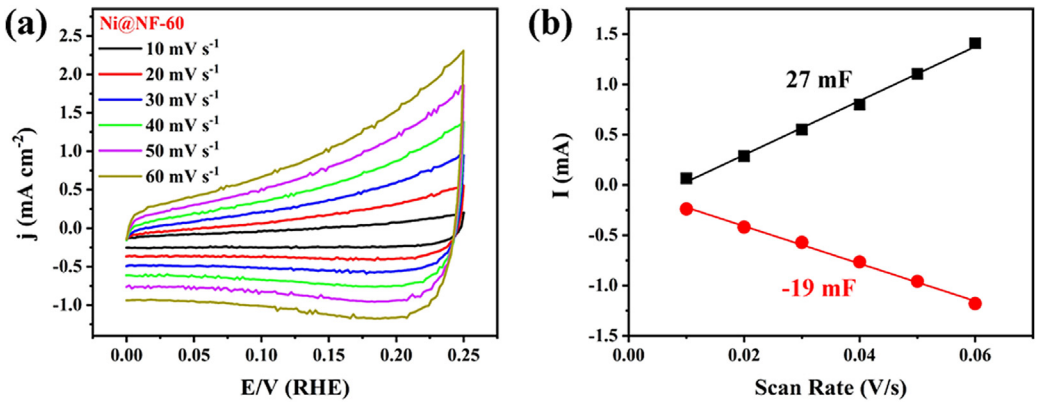

Fig. 8 – Electrochemically active surface area (ECSA) measurements of Ni@NF-60 catalyst. (a) CV profiles measured at different scan rates from 10 to 60 mV/s in the non-Faradic region. (b) Cathodic and anodic charging current measured at 1.17 V vs. RHE plotted as a function of scan rate for double-layer capacitance measurement.

higher current density (1000 mA/cm^{-2}) as depicted in chronopotentiometry response provided in supplementary material (Fig. S2). After long-term chronopotentiometry test, the polarization curve of Ni@NF-60 electrode was re-evaluated and compared with the response before the stability test, as shown in Fig. 7(d). The polarization curve after the stability test showed consistent behavior with its fresh form, indicating the stable configuration of the electrode after long term OER activity.

Moreover, electrochemically active surface area (ECSA) of the best performing catalyst (Ni@NF-60) was calculated using following relationship:

$$ESCA = \frac{C_{DL}}{C_S}$$

Here, C_s implies the specific capacitance of the metal electrodes which is reported to be 0.04 cm^2 for alkaline electrolyte [52]. To measure the double-layer capacitance (C_{DL}), continuous CVs of varying scan rates from 10 to 60 mV/s were performed in non-Faradaic regions as shown in Fig. 8(a). The current density (j) is directly proportional with the scan rate. The C_{DL} was determined by averaging the cathodic and anodic slopes of the plots of the current versus scan rate, as shown in Fig. 8(b). The ECSA of Ni@NF-60 is calculated to be 264 cm^2.

The OER activity of a catalyst is influenced by many factors, among which the structural property of the catalyst plays an important role. The crystallinity or amorphization, porosity and specific morphology define the structural character of the catalyst. The difference in OER performance of as-synthesized nickel electrocatalysts can be understood based on the SEM morphology presented in Fig. (2). The better performance of the Ni@NF-60 catalyst is attributed to the formation of snowflakes like morphology (Fig. 2(f)), which are porous and fluffy compared to other two analogs, Ni@NF-30 and Ni@NF-60, with the former having an underdeveloped morphology (Fig. 2(d)), while the latter have a dense and compact morphology (Fig. 2 (d)). The porous structure adsorbs more hydroxyl ions (OH^-) and the snowflake like structure of the catalyst presents highly active catalytic sites that accelerate the OER reaction kinetics, and thus high current density at low-overpotential value is observed for Ni@NF-60 catalyst.

The OER performance of AACVD thin film catalyst is evaluated by comparing it with other Ni catalysts synthesized by different methods as well as the commercially available noble metal (Ir and Ru oxide) benchmark catalysts, as shown in Table 1. The thin film catalysts prepared in 60 min of AACVD process clearly demonstrates low overpotential to obtain 10 mA/cm^2 and have ability to approach higher current density of 1000 mA/cm^2. This ability is lacking in other catalysts. The high OER activity is attributed to nanoscale features of Ni deposited on the surface of porous nickel foam. Furthermore, the synergy created between highly conductive nickel foam

Table 1 – Comparative analysis of different nickel oxide thin films and noble metal electrocatalysts prepared from different procedures for water oxidation reaction.

Catalyst/System[a]	Support	Synthetic strategy	Potential [mV]@10 mA/cm^2	Peak current density mA/cm^2	Tafel slope [mV dec^{-1}]	Ref.
Ni@NF-60	NF[b]	AACVD[c]	285	>1000	73	This work
Mesoporous NiO	NF	Hydrothermal method	335	300	120	[57]
NiO_x film	NF	Electrodeposition	375	>300	68	[58]
NiO_x	NF	Sol–gel	358	>150	78	[59]
NiO	NF	Thermal oxidation	310	100	54	[60]
$NiMoO_4$	NF	AACVD	310	>175	82	[61]
IrO_2	Glass carbon	Commercial	301	>170	75	[62]
RuO_2	NF	Commercial	322	400	55	[63]

and nanostructured nickel catalyst favors fast electronic transport between electrode/electrocatalyst interfaces. The simple and straightforward fabrication strategy adopted in this work is highly attractive for the up-scaling of the electrocatalyst. Thus, the low-cost nickel film obtained through inexpensive AACVD using simple chemical precursor is fascinating than the other synthesis approaches, where the reproducibility and performance might be a challenge.

Moreover, the OER activity of the Ni thin-film electrocatalyst was monitored several times and the results proved to be reproducible and consistent. This is attributed to the simple and easy-to-use AACVD approach, which has the ability to replicate thin-film electrodes with similar structural properties with high certainty. Post SEM/EDX analyses of the Ni@NF-60 catalyst was performed to understand the morphological and compositional changes due to long-term OER testing. The SEM images (Fig. S3 (a)–(b)) showed the preservation of nanoscale features on the catalyst surface. It is worth noting that the catalyst was initially comprised of metallic nickel only (Fig. S1) and had no oxygen, prior to the OER. However, during the water oxidation process in 1.0 KOH, catalyst, catalyst attained a significant amount of oxygen (Fig. S3(c)), which is attributed to the oxidation of Ni to NiO. This type of phase change has often been observed in the earlier literature on electrochemical water oxidation [49,56].

Conclusions

In this study, a simple one-step chemical vapor deposition process was developed to fabricate nanostructured nickel-based thin-film electrocatalysts with convincing propensity for water oxidation. The catalyst shows good oxygen evolution activity, exhibiting a low overpotential of 285 mV at 10 mA/cm^2 and a high current density of 1000 mA/cm^2 at 1.6 V (overpotential of 423 mV). The as-developed nano-electrocatalyst remained stable for at least 20 h. The low Tafel slope of 73 mV/decade also indicates good kinetics for electrocatalytic water oxidation. The results are important for the development of non-precious metal catalytic materials for solar water-splitting devices. The high activity and excellent stability under favorable conditions suggest that more active water oxidation catalysts can be obtained by modifying the structure of the molecular precursors.

Declaration of competing interest

The authors declare that they have no known competing financial interests or personal relationships that could have appeared to influence the work reported in this paper.

Acknowledgment

Authors acknowledge the research facilities provided by the Interdisciplinary Research Center for Hydrogen and Energy Storage (IRC-HES) at King Fahd University of Petroleum and Minerals (KFUPM).

Appendix A. Supplementary data

Supplementary data to this article can be found online at https://doi.org/10.1016/j.ijhydene.2023.01.083.

REFERENCES

[1] You B, Sun Y. Innovative strategies for electrocatalytic water splitting. Acc Chem Res 2018;51:1571–80.
[2] Lee JE, Jeon K-J, Show PL, Jung S-C, Choi YJ, Rhee GH, et al. Mini review on H2 production from electrochemical water splitting according to special nanostructured morphology of electrocatalysts. Fuel 2022;308:122048.
[3] Abdin Z, Zafaranloo A, Rafiee A, Merida W, Lipinski W, Khalilpour KR. Hydrogen as an energy vector. Renew Sustain Energy Rev 2020;120:109620.
[4] Yu M, Wang K, Vredenburg H. Insights into low-carbon hydrogen production methods: green, blue and aqua hydrogen. Int J Hydrogen Energy 2021;46:21261–73.
[5] Abbas HF, Daud WW. Hydrogen production by methane decomposition: a review. Int J Hydrogen Energy 2010;35:1160–90.
[6] Lai C-C, Shih T-P, Ko W-C, Tang H-J, Hsueh P-R. Severe acute respiratory syndrome coronavirus 2 (SARS-CoV-2) and coronavirus disease-2019 (COVID-19): the epidemic and the challenges. Int J Antimicrob Agents 2020;55:105924.
[7] Yu ZY, Duan Y, Feng XY, Yu X, Gao MR, Yu SH. Clean and affordable hydrogen fuel from alkaline water splitting: past, recent progress, and future prospects. Adv Mater 2021;33:2007100.
[8] Anwar S, Khan F, Zhang Y, Djire A. Recent development in electrocatalysts for hydrogen production through water electrolysis. Int J Hydrogen Energy 2021;46:32284–317.
[9] Song J, Wei C, Huang Z-F, Liu C, Zeng L, Wang X, et al. A review on fundamentals for designing oxygen evolution electrocatalysts. Chem Soc Rev 2020;49:2196–214.
[10] Li Y, Zhou L, Guo S. Noble metal-free electrocatalytic materials for water splitting in alkaline electrolyte. Energy 2021;3:100053.
[11] Ehsan MA, Adam A, Rehman A, Hakeem AS, Isab AA, Qamar M. Morphologically controlled rapid fabrication of rhodium sulfide (Rh 2 S 3) thin films for superior and robust hydrogen evolution reaction. Sustain Energy Fuels 2021;5:459–68.
[12] Ehsan MA, Adam A, Rehman A, Qamar M. Direct self-assembly of hierarchically grown rhodium thin films for electrocatalytic hydrogen evolution reaction. Catalysts 2021;11:338.
[13] Ehsan MA, Suliman MH, Rehman A, Hakeem AS, Al Ghanim A, Qamar M. Fabrication of platinum thin films for ultra-high electrocatalytic hydrogen evolution reaction. Int J Hydrogen Energy 2020;45:15076–85.
[14] Ehsan MA, Suliman MH, Rehman A, Hakeem AS, Yamani ZH, Qamar M. Direct deposition of a nanoporous palladium electrocatalyst for efficient hydrogen evolution reaction. New J Chem 2020;44:7795–801.
[15] Audichon T, Napporn TW, Canaff C, Cu Morais, Comminges Cm, Kokoh KB. IrO2 coated on RuO2 as efficient and stable electroactive nanocatalysts for electrochemical water splitting. J Phys Chem C 2016;120:2562–73.
[16] Hunter BM, Gray HB, Muller AM. Earth-abundant heterogeneous water oxidation catalysts. Chem Rev 2016;116:14120–36.

[17] Han L, Dong S, Wang E. Transition-metal (Co, Ni, and Fe)-based electrocatalysts for the water oxidation reaction. Adv Mater 2016;28:9266–91.
[18] Feng Y, Yang H, Wang X, Hu C, Jing H, Cheng J. Role of transition metals in catalyst designs for oxygen evolution reaction: a comprehensive review. Int J Hydrogen Energy 2022;47:17946–70.
[19] Nozari-Asbemarz M, Amiri M, Imanzadeh H, Bezaatpour A, Nouhi S, Hosseini P, et al. Mixed metal oxides as efficient electrocatalysts for water oxidation. Int J Hydrogen Energy 2022;47:5250–9.
[20] De S, Zhang J, Luque R, Yan N. Ni-based bimetallic heterogeneous catalysts for energy and environmental applications. Energy Environ Sci 2016;9:3314–47.
[21] Angeles-Olvera Z, Crespo-Yapur A, Rodriguez O, Cholula-Diaz JL, Martinez LM, Videa M. Nickel-based electrocatalysts for water electrolysis. Energies 2022;15:1609.
[22] Yan X, Zhang W-D, Hu Q-T, Liu J, Li T, Liu Y, et al. Defects-rich nickel nanoparticles grown on nickel foam as integrated electrodes for electrocatalytic oxidation of urea. Int J Hydrogen Energy 2019;44:27664–70.
[23] El-Maghrabi HH, Nada AA, Roualdes S, Bekheet MF. Design of Ni/NiO–TiO2/rGO nanocomposites on carbon cloth conductors via PECVD for electrocatalytic water splitting. Int J Hydrogen Energy 2020;45:32000–11.
[24] Hameed RA, Medany SS. Enhanced electrocatalytic activity of NiO nanoparticles supported on graphite planes towards urea electro-oxidation in NaOH solution. Int J Hydrogen Energy 2017;42:24117–30.
[25] Kumar JP, Giri SD, Sarkar A. Mesoporous NiO with different morphology: synthesis, characterization and their evaluation for oxygen evolution reaction. Int J Hydrogen Energy 2018;43:15639–49.
[26] Yu X, Xu P, Hua T, Han A, Liu X, Wu H, et al. Multi-walled carbon nanotubes supported porous nickel oxide as noble metal-free electrocatalysts for efficient water oxidation. Int J Hydrogen Energy 2014;39:10467–75.
[27] Beliaeva K, Grimaldos-Osorio N, Ruiz-Lopez E, Burel L, Vernoux P, Caravaca A. New insights into lignin electrolysis on nickel-based electrocatalysts: electrochemical performances before and after oxygen evolution. Int J Hydrogen Energy 2021;46:35752–64.
[28] Narwade SS, Mali SM, Digraskar RV, Sapner VS, Sathe BR. Ni/NiO@ rGO as an efficient bifunctional electrocatalyst for enhanced overall water splitting reactions. Int J Hydrogen Energy 2019;44:27001–9.
[29] Cheng N, Liu Q, Tian J, Sun X, He Y, Zhai S, et al. Nickel oxide nanosheets array grown on carbon cloth as a high-performance three-dimensional oxygen evolution electrode. Int J Hydrogen Energy 2015;40:9866–71.
[30] Silva VD, Raimundo RA, Simoes TA, Loureiro FJ, Fagg DP, Morales MA, et al. Nonwoven Ni–NiO/carbon fibers for electrochemical water oxidation. Int J Hydrogen Energy 2021;46:3798–810.
[31] Liu M, Sun Y-Y, Zhu Y-X, Wu L-K, Jiang M-Y, Hou G-Y, et al. Selenium doped nickel nanosheet array for oxygen evolution reaction. Int J Hydrogen Energy 2021;46:6427–40.
[32] Qiu Z, Ma Y, Edstrom K, Niklasson GA, Edvinsson T. Controlled crystal growth orientation and surface charge effects in self-assembled nickel oxide nanoflakes and their activity for the oxygen evolution reaction. Int J Hydrogen Energy 2017;42:28397–407.
[33] Sahoo P, Sharma A, Padhan S, Thangavel R. Cu doped NiO thin film photocathodes for enhanced PEC performance. Superlattice Microst 2021;159:107050.
[34] He L, Zhou W, Cai D, Mao SS, Sun K, Shen S. Pulsed laser-deposited n-Si/NiO x photoanodes for stable and efficient photoelectrochemical water splitting. Catal Sci Technol 2017;7:2632–8.
[35] Lee SA, Lee TH, Kim C, Lee MG, Choi M-J, Park H, et al. Tailored NiO x/Ni cocatalysts on silicon for highly efficient water splitting photoanodes via pulsed electrodeposition. ACS Catal 2018;8:7261–9.
[36] Sun K, Saadi FH, Lichterman MF, Hale WG, Wang H-P, Zhou X, et al. Stable solar-driven oxidation of water by semiconducting photoanodes protected by transparent catalytic nickel oxide films. Proc Natl Acad Sci USA 2015;112:3612–7.
[37] Mat Teridi M, Tahir AA, Senthilarasu S, Wijayantha K, Sulaiman M, Ahmad Ludin N, et al. Fabrication of NiO photoelectrodes by aerosol-assisted chemical vapour deposition (AACVD). Phys Status Solidi Rapid Res Lett 2014;8:982–6.
[38] Saddiqa A, Nisar L, Gilani SR, Joya KS. Surface-assembled non-noble metal nanoscale Ni-colloidal thin-films as efficient electrocatalysts for water oxidation. RSC Adv 2019;9:37274–86.
[39] Kou T, Wang S, Hauser JL, Chen M, Oliver SR, Ye Y, et al. Ni foam-supported Fe-doped β-Ni (OH) 2 nanosheets show ultralow overpotential for oxygen evolution reaction. ACS Energy Lett 2019;4:622–8.
[40] Duan J-J, Zhang R-L, Feng J-J, Zhang L, Zhang Q-L, Wang A-J. Facile synthesis of nanoflower-like phosphorus-doped Ni3S2/CoFe2O4 arrays on nickel foam as a superior electrocatalyst for efficient oxygen evolution reaction. J Colloid Interface Sci 2021;581:774–82.
[41] Zhang L, Ma Y-T, Duan J-J, Yao Y-Q, Feng J-J, Wang A-J. In-situ construction of 3D hetero-structured sulfur-doped nanoflower-like FeNi LDH decorated with NiCo Prussian blue analogue cubes as efficient electrocatalysts for boosting oxygen evolution reaction. J Colloid Interface Sci 2022;611:205–14.
[42] Duan J-J, Han Z, Zhang R-L, Feng J-J, Zhang L, Zhang Q-L, et al. Iron, manganese co-doped Ni3S2 nanoflowers in situ assembled by ultrathin nanosheets as a robust electrocatalyst for oxygen evolution reaction. J Colloid Interface Sci 2021;588:248–56.
[43] Ehsan MA, Rehman A. Facile and scalable fabrication of nanostructured nickel thin film electrodes for electrochemical detection of formaldehyde. Anal Methods 2020;12:4028–36.
[44] Ehsan MA, Hakeem AS, Rehman A. Synergistic effects in bimetallic Pd–CoO electrocatalytic thin films for oxygen evolution reaction. Sci Rep 2020;10:1–11.
[45] Ehsan MA, Shah SS, Basha SI, Hakeem AS, Aziz MA. Recent advances in processing and applications of heterobimetallic oxide thin films by aerosol-assisted chemical vapor deposition. Chem Rec 2021;22:e202100278.
[46] Grosvenor AP, Biesinger MC, Smart RSC, McIntyre NS. New interpretations of XPS spectra of nickel metal and oxides. Surf Sci 2006;600:1771–9.
[47] Nesbitt H, Legrand D, Bancroft G. Interpretation of Ni2p XPS spectra of Ni conductors and Ni insulators. Phys Chem Miner 2000;27:357–66.
[48] Ehsan MA, Rehman A, Afzal A, Ali A, Hakeem AS, Akbar UA, et al. Highly effective electrochemical water oxidation by millerite-phased nickel sulfide nanoflakes fabricated on Ni foam by aerosol-assisted chemical vapor deposition. Energy Fuels 2021;35:16054–64.
[49] Ehsan MA, Khan A, Zafar MN, Akber UA, Hakeem AS, Nazar MF. Aerosol-assisted chemical vapor deposition of nickel sulfide nanowires for electrochemical water oxidation. Int J Hydrogen Energy 2022;47:42001–12.
[50] Khan A, Hakeem AS, Mohamed HD, Al-Saeed MHA, Ehsan MA. NiPd nano-alloy film as a promising low

overpotential electrocatalyst for high activity water oxidation reaction. J Environ Chem Eng 2022;10:107959.
[51] Babar N-U-A, Hakeem AS, Ehsan MA. Direct fabrication of nanoscale NiVO x electrocatalysts over nickel foam for a high-performance oxygen evolution reaction. ACS Appl Energy Mater 2022;5:4318–28.
[52] McCrory CC, Jung S, Peters JC, Jaramillo TF. Benchmarking heterogeneous electrocatalysts for the oxygen evolution reaction. J Am Chem Soc 2013;135:16977–87.
[53] Damjanovic A, Dey A, Jo 'MB. Kinetics of oxygen evolution and dissolution on platinum electrodes. Electrochim Acta 1966;11:791–814.
[54] Song F, Hu X. Exfoliation of layered double hydroxides for enhanced oxygen evolution catalysis. Nat Commun 2014;5:1–9.
[55] Shinagawa T, Garcia-Esparza AT, Takanabe K. Insight on Tafel slopes from a microkinetic analysis of aqueous electrocatalysis for energy conversion. Sci Rep 2015;5:1–21.
[56] Inamdar AI, Chavan HS, Hou B, Lee CH, Lee SU, Cha S, et al. A robust nonprecious CuFe composite as a highly efficient bifunctional catalyst for overall electrochemical water splitting. Small 2020;16:1905884.
[57] Wu Z, Vagin M, Boyd R, Bakhit B, Greczynski G, Oden M, et al. Morphology effects on electrocatalysis of anodic water splitting on nickel (II) oxide. Microporous Mesoporous Mater 2022;333:111734.
[58] He C, Wu X, He Z. Amorphous nickel-based thin film as a Janus electrocatalyst for water splitting. J Phys Chem C 2014;118:4578–84.
[59] Noguera Gomez J, Garcia Tecedor M, Sanchez Royo JF, Valencia Linan LM, de la Mata M, Herrera-Collado M, et al. Solution-processed Ni-based nanocomposite electrocatalysts: an approach to highly efficient electrochemical water splitting. ACS Appl Energy Mater 2021;4:5255–64.
[60] Babar P, Lokhande A, Gang M, Pawar B, Pawar S, Kim JH. Thermally oxidized porous NiO as an efficient oxygen evolution reaction (OER) electrocatalyst for electrochemical water splitting application. J Ind Eng Chem 2018;60:493–7.
[61] Ehsan MA, Khan A. Aerosol-assisted chemical vapor deposition growth of NiMoO4 nanoflowers on nickel foam as effective electrocatalysts toward water oxidation. ACS Omega 2021;6:31339–47.
[62] Lin Y, Zhou S, Sheehan SW, Wang D. Nanonet-based hematite heteronanostructures for efficient solar water splitting. J Am Chem Soc 2011;133:2398–401.
[63] Zhu Y-X, Jiang M-Y, Liu M, Wu L-K, Hou G-Y, Tang Y-P. An Fe–V@ NiO heterostructure electrocatalyst towards the oxygen evolution reaction. Nanoscale 2020;12:3803–11.